Ion Permeation and Block of M-Type and Delayed Rectifier Potassium Channels

Whole-Cell Recordings from Bullfrog Sympathetic Neurons

BRIAN M. BLOCK* and STEPHEN W. JONES‡

From the Departments of *Neurosciences and ‡Physiology and Biophysics, Case Western Reserve University, Cleveland, Ohio 44106

ABSTRACT Ion permeation and conduction were studied using whole-cell recordings of the M-current (I_M) and delayed rectifier (I_{DR}), two K^+ currents that differ greatly in kinetics and modulation. Currents were recorded from isolated bullfrog sympathetic neurons with 88 mM $[K^+]_i$ and various external cations. Selectivity for extracellular monovalent cations was assessed from permeability ratios calculated from reversal potentials and from chord conductances for inward current. P_{Rb}/P_K was near 1.0 for both channels, and G_{Rb}/G_K was 0.87 ± 0.01 for I_{DR} but only 0.35 ± 0.01 for I_M (15 mM $[Rb^+]_o$ or $[K^+]_o$). The permeability sequences were generally similar for I_M and I_{DR}: $K^+ \sim Rb^+ > NH_4^+ > Cs^+$, with no measurable permeability to Li^+ or $CH_3NH_3^+$. However, Na^+ carried detectable inward current for I_{DR} but not I_M. Na_o^+ also blocked inward K^+ current for I_{DR} (but not I_M), at an apparent electrical distance (δ) ~0.4, with extrapolated dissociation constant (K_D) ~1 M at 0 mV. Much of the instantaneous rectification of I_{DR} in physiologic ionic conditions resulted from block by Na_o^+. Extracellular Cs^+ carried detectable inward current for both channel types, and blocked I_M with higher affinity (K_D = 97 mM at 0 mV for I_M, K_D ~0.2 M at 0 mV for I_{DR}), with δ ~0.9 for both. I_{DR} showed several characteristics reflecting a multi-ion pore, including a small anomalous mole fraction effect for P_{Rb}/P_K, concentration-dependent G_{Rb}/G_K, and concentration-dependent apparent K_D's and δ's for block by Na_o^+ and Cs_o^+. I_M showed no clear evidence of multi-ion pore behavior. For I_M, a two-barrier one-site model could describe permeation of K^+ and Rb^+ and block by Cs_o^+, whereas for I_{DR} even a three-barrier, two-site model was not fully adequate.

INTRODUCTION

Despite the great kinetic and functional diversity of K^+ channels, the permeation properties of K^+ channels are generally similar (Hille, 1992). It has long been recognized that permeation in K^+ channels must reconcile two apparently contradictory properties, a high rate of ion conduction and yet a high selectivity among similar ions. A single-file, multi-ion pore with specific binding sites has been the preferred model to explain these properties (Hille and Schwartz, 1978). Hallmarks of multi-ion pores include flux ratio exponents >1.0 (Hodgkin and Keynes, 1955), concentration-dependent permeability ratios (Perez-Cornejo and Begenisich, 1994), anomalous mole fraction effects in mixtures of permeant ions (Hagiwara et al., 1977; Wagoner and Oxford, 1987; Heginbotham and MacKinnon, 1993), and concentration dependence of the apparent voltage dependence of channel block (Adelman and French, 1978; French and Shoukimas, 1985).

We have studied ion permeation and block using whole-cell recordings of two K^+ currents of frog sympathetic neurons, M-current (I_M) and delayed rectifier (I_{DR}). These currents differ greatly in properties other than permeation. Half activation ($V_{1/2}$) is near −35 mV for I_M versus 0 mV for I_{DR}, and the activation time constant at $V_{1/2}$ is ~10-fold slower for I_M than for I_{DR} (Adams et al., 1982*a*). I_{DR} inactivates slowly (seconds), whereas I_M is completely noninactivating (Adams et al., 1982*a*), which is unusual among voltage-dependent K^+ currents. In addition, several neurotransmitters inhibit I_M (Jones and Adams, 1987), without detectable effect on I_{DR} (Adams et al., 1982*b*). I_M and I_{DR} channels are clearly K^+ selective (Adams et al., 1982*a*), but their per-

Address correspondence to Brian M. Block, Department of Neurosciences, Case Western Reserve University, Cleveland, Ohio 44106. Fax: (216) 368-3952; E-mail: bmb5@po.cwru.edu

 J. GEN. PHYSIOL. © The Rockefeller University Press • 0022-1295/96/04/473/16 $2.00
Volume 107 April 1996 473–488

meation mechanisms have not been described in detail.

Ionic selectivity for I_M and I_{DR} channels was evaluated by measuring relative permeabilities and conductances for K^+, Rb^+, NH_4^+, Cs^+, Na^+, Li^+, and $CH_3NH_3^+$. The ability of extracellular Na^+ and Cs^+ to block inward K^+ current through each channel was also determined. Both I_M and I_{DR} were tested for anomalous mole fraction effects in mixtures of Rb_o^+ and K_o^+. Barrier/well models using Eyring rate theory were developed. The ability to compare permeation properties of two K^+ channels under nearly identical conditions allowed each channel to serve as an internal control for the other. Preliminary results of this project have been reported (Block and Jones, 1995).

MATERIALS AND METHODS

Cells and Recording Conditions

Neurons were isolated as previously described (Kuffler and Sejnowski, 1983; Jones, 1987). Briefly, caudal paravertebral sympathetic ganglia were dissected from adult bullfrogs and enzymatically dissociated. Isolated neurons were stored in supplemented L15 culture media at 4°C. Large spherical neurons (55.6 ± 2.3 pF; range 14–93 pF) were used for recordings. Patch clamp recordings were made at room temperature (22–24°C) in the whole cell configuration (Hamill et al., 1981). Electrodes were pulled from 7052 or EN-1 glass (Garner Glass, Claremont, CA) with resistance 1.5–2.5 MΩ. Series resistances (R_S) in the whole-cell configuration, estimated from optimal correction of the capacity transient, were 2–4 MΩ. R_S compensation was 80% for I_M and >90% for I_{DR}. For 0.4 MΩ of uncompensated series resistance, the steady-state voltage error would be 0.4 mV/nA, and the time constant of the voltage clamp would be 22 μs for a 55-pF cell. Voltages shown in the figures are the voltage commands.

Currents were recorded with an Axopatch 200 amplifier, Labmaster A-D interface, and 8-pole Bessel low-pass filter, and stored on a personal computer. The sampling frequency was 1–10 kHz for I_M with 0.3–3 kHz analogue filtering, and 10 kHz for I_{DR} with 3-kHz analogue filtering. pClamp software (Clampex, Axon Instruments, Foster City, CA) was used for data acquisition.

Solutions

The standard intracellular solution was (mM): 60 KCl, 8 KOH, 10 K_2EGTA, 4 $MgCl_2$, 2.5 N-methyl-D-glucamine (NMG)-HEPES, 0.3 Li_2-GTP, 3 $CaCl_2$, 5 TRIS-ATP, 14 TRIS-phosphocreatine, pH 7.2. Free Ca^{2+} was estimated at 70 nM using the FREECA program (Fabiato and Fabiato, 1979). In some I_M experiments Na-HEPES replaced NMG-HEPES; no differences were observed between currents in the two solutions. For some measurements of I_{DR} activation curves (see Results), KCl was reduced to 25 mM, with addition of 35 mM NMG-Cl (and replacement of K_2EGTA and KOH with NMG_2EGTA and NMG base). Otherwise, the intracellular solution was not varied. The standard extracellular solution for I_M was 115 NaCl, 2.5 KCl, 2.5 Na-HEPES, 2 $MnCl_2$. For I_{DR} experiments, extracellular Na^+ was replaced with NMG^+, except for Figs. 1, *A–C*, 8, and 9, where the effects of extracellular Na^+ were tested. Different extracellular solutions are noted in the text. In all variations on these solutions, ionic strength was held constant. Chemicals were purchased from Sigma Chemical Co. (St. Louis, MO), except for saxitoxin (Calbiochem, La Jolla, CA) and tetraethylammonium chloride (TEA; Eastman Laboratory Chemical, Rochester, NY).

Extracellular solutions were changed by a "sewer pipe" fast flow system, unless noted otherwise. The pipes were deactivated fused silica tubing (0.32 mm inner diameter, J&W Scientific, Folsom, CA) held together with Sylgard (Dow Corning, Midland, MI). Cells were placed within 100 μm of the pipe opening. Previous studies have shown complete and rapid solution exchange with this type of flow system (Jones, 1991; Thévenod and Jones, 1992).

Current Isolation

I_M was isolated by holding the cell depolarized at −30 mV, which partially inactivated Na^+ current and other K^+ currents (Adams et al., 1982*a*). I_M ran up over time because of the ATP regenerating system in the intracellular solution. No measurements were made on I_M until the current became stable, which required ~10 min of whole-cell dialysis. I_M rundown was negligible over the next hour of recording (~80% of current remained). In some cells, return to −30 mV from strongly hyperpolarized voltages triggered a K^+ current that activated over tens of milliseconds and then inactivated over several seconds. That current resembled the "slow A-current" (I_{SA}) reported by Selyanko et al. (1990). When I_{SA} was observed, the time between steps was increased to allow full inactivation of I_{SA} (incomplete inactivation was visible as an increase in the outward holding current at −30 mV). I_{SA} is routinely observed under conditions in which I_M shows rapid rundown (e.g., absence of intracellular ATP), but only occasionally in the experiments reported here. Recording was halted if I_{SA} became large enough to interfere with measurement of I_M. With these precautions to exclude I_{SA}, only I_M and a linear leak were present in the voltage range up to −30 mV (Adams et al., 1982*a*; Jones, 1989). Isolation of I_M was confirmed by the observation that 96 ± 3% (n = 6) of the relaxation from −30 mV was inhibited by 100 nM chicken II LHRH. At more positive voltages, separation of I_M and I_{DR} required tail current analysis; see below.

I_{DR} experiments were performed from a −60 mV holding potential. I_{DR} was isolated by replacing Na^+ in the extracellular solution with NMG^+, and by replacement of extracellular Ca^{2+} with Mn^{2+} to prevent Ca^{2+}-dependent K^+ currents. Where Na^+-containing solutions were used (Figs. 1, *A–C*, 8, and 9), the 75–90-ms step to +10 mV, given to activate I_{DR}, inactivated Na^+ current before measurements or hyperpolarizing steps were made. I_{DR} was far larger than I_M, so contamination of I_{DR} tails with I_M was minimal (~10%, based on comparison of mean chord conductances). I_{DR} did not display ATP-dependent run-up, but measurements were delayed until the current amplitude stabilized (~5 min).

Analysis

Currents were analyzed using pClamp (Clampan 5.5 and Clampfit 6.0) and Excel 5.0 (Microsoft Corp., Redmond, WA). Activation, ionic block, and Eyring rate theory models were fitted with the Solver function of Excel, which uses a generalized reduced gradient method to optimize the parameters. Goodness of fit was determined by minimizing the sum of the squared errors.

Differences among experimental conditions were evaluated by two-tailed Student's t tests, using Bonferroni correction for multiple tests, with $P < 0.05$ considered to be significant. Values presented are means ± SEM.

For all measurements involving changes in extracellular solutions, test conditions were compared with measurements made both before and after the test. The control value was then defined as the average of measurements before and after.

Permeabilities and conductances. Ion selectivity was assessed under conditions in which the extracellular solution contained only a single permeant ion at a time. I_{DR} permeability ratios were determined in extracellular solutions in which the only cations were Mn^{2+}, NMG^+, and the ion of interest (either X^+ + NMG^+, or 120 mM X^+). For I_M, where Na^+ was not permeable (see Fig. 7), extracellular solutions contained Na^+ rather than NMG^+. Reversal potentials (E_{REV}) and conductances were determined from the protocols of Fig. 1, *A* and *B*, unless noted otherwise. Permeability ratios (P_X/P_K) were calculated from the shift in E_{REV} between solutions, using a version of the Goldman-Hodgkin-Katz voltage equation (Eqs. 13–17 of Hille, 1992):

$$\Delta E_{REV} = (RT/F) \ln \{ (P_X [X]_o) / (P_K [K]_o) \} . \quad (1)$$

Chord conductances were defined from

$$I_X = G_X (V - E_{REV}) \quad (2)$$

and were calculated from "instantaneous" currents, generally measured at −100 mV. Conductance measurements were made at −110 mV for data in 2.5 mM K_o^+ or Rb_o^+, at −120 mV for data in 120 mM Na_o^+, and at −80 mV in NH_{4o}^+ or Cs_o^+. Those voltages were at least 25 mV negative to E_{REV} in each ionic condition, except for Na_o^+, where E_{REV} was extremely negative, −103.9 ± 0.8 mV (n = 17). By using measurements made far from E_{REV}, the chord conductances reflect primarily ion influx through the pore. From the Goldman-Hodgkin-Katz current equation, we estimate that influx is 2.7-fold larger than efflux at 25 mV negative to reversal; for Eyring models (e.g., Fig. 12), ratios were 2.7 to 6.2, depending on the parameters and ion concentrations.

I_M. I_M measurements were made on leak-subtracted currents. Leak subtraction was not straightforward, as I_M was usually measured from a holding potential of −30 mV where there was significant resting I_M. Two methods were used for leak subtraction, "method 1" for chord conductances, and "method 2" for E_{REV}. In method 1, leak current was measured from a linear fit to the steady-state current negative to −80 mV (Jones, 1989). Steady-state currents were measured at the end of each tail current (average current between 0.9 to 1.0 s). I_M amplitude was then defined by the instantaneous current, the average current between 5 and 10 ms after repolarization, minus the linear leak (e.g., Fig. 4 *A*). Empirical single exponential fits to I_M relaxations indicated that measurement at 5 to 10 ms may have underestimated the I_M amplitude by 28% in 2.5 mM K_o^+ at −110 mV and 16% in 15 mM K_o^+ at −100 mV. Because the time constants for I_M relaxations did not vary between K_o^+ and Rb_o^+, that underestimation would not affect the relative conductances.

In method 2, I_M records were leak-subtracted by changing the holding potential to −80 mV and giving hyperpolarizing steps of one-half amplitude, with two to four records averaged and scaled. E_{REV} for I_M was measured from the leak-subtracted records as the point of zero relaxation, either from the intersection of the instantaneous and steady-state currents, or by fitting each tail current to a single exponential function and taking the zero amplitude point as E_{REV}. I_M records in the figures are either subtracted by method 2, or unsubtracted (as noted), with 5 ms blanked on each voltage step.

I_{DR}. I_{DR} currents were leak subtracted using inverted steps of one-fourth amplitude, with four records averaged and scaled. Instantaneous I–V relations were measured from tail current amplitudes, averaged between 0.5–0.6 and 1 ms after repolarization. I_{DR} records shown in the figures have 0.5–0.6 ms blanked on each change in voltage.

Activation curves. The dependence of channel opening on voltage was determined from tail currents recorded at −60 mV, after depolarizations of variable amplitude. That required voltage steps that activated both I_M and I_{DR}, which were separated using tail current analysis. Tail currents were fitted to the sum of two exponential components (using Clampfit), with the time constant (τ) of each fixed to values estimated for I_M and I_{DR} separately. For I_M, τ was measured from the single exponential relaxation at −60 mV from the −30 mV holding potential. For I_{DR}, τ was measured from the fast component of the tail at −60 mV after a 1-s step to +30 mV. The τ was ~10-fold faster than for I_{DR} than for I_M. I_M activation was then defined from the amplitude of the slow component. Because of the large amplitude of I_{DR} tails, the protocol was run twice, recording currents at high gain to measure the predominantly I_M tails in the −100 to −20 mV range, and again at lower gain for tails above −20 mV. Occasionally, there appeared to be a slow component to I_{DR} tails, 2–6% of the total tail current amplitude after steps from +30 to +50 mV. To avoid contamination of I_M tail measurements by a slow I_{DR} component, I_M activation was measured only up to 0 mV, and values were included only if the slow component was estimated to be at least 80% I_M. I_M tails were fitted to a Boltzmann relation:

$$I_M = I_{M,max} / \{ 1 + \exp [z F (V_{1/2} - V) / (RT)] \} + I_{M,0} . \quad (3)$$

The Solver from Excel was used to estimate z, $V_{1/2}$, $I_{M,max}$, and $I_{M,0}$. The $I_{M,0}$ term was needed because there was a small amount of I_M activation at −60 mV, so "tail" amplitudes from more negative voltages have reversed sign.

Junction potentials. Before forming a seal with the membrane, the patch pipette current was manually adjusted to zero with the normal extracellular solution in the bath and an Ag/AgCl pellet electrode in the bath as reference. In the whole-cell configuration, solution changes were made with a flow pipe system, with the outflow of the pipes directed away from the Ag/AgCl pellet. Under those conditions, there were two sources of junction potentials: the electrode-bath interface, and the boundary between the bath and the solution flowing from a pipe (Barry and Lynch, 1991; Neher, 1992). Once a seal was formed, the potential from the electrode-bath junction produced an offset from true zero voltage for the remainder of the experiment.

Junction potentials were measured with the amplifier in current clamp mode, using a patch pipette filled with 3 M KCl as reference, and a patch pipette filled with the intracellular solution as the sensing electrode. The pipette current was set to zero with the bath also containing the intracellular solution (see Neher, 1992). The voltage was then recorded on changing the bath to each extracellular solution, with a second measurement in the initial (zero junction potential) conditions to reduce errors caused by drift. In the standard polarity convention (Barry and

Lynch, 1991; Neher, 1992), the junction potential is the negative of the recorded voltage. Junction potentials were +4.9 to +6.2 mV for K^+ or Rb^+ with Na^+ solutions and +10.6 to +13.6 mV for K^+ or Rb^+ with NMG^+ solutions. Junction potentials did not vary between K^+ and Rb^+ solutions and were generally consistent with previous calculated and measured values (Barry and Lynch, 1991; Neher, 1992).

For solutions containing 120 mM Na^+, NH_4^+ or Cs^+, junction potentials were measured using the flow pipe apparatus. The bath was filled with 2.5 mM K^+ plus 117.5 mM Na^+, and an electrode filled with 3 M KCl was zeroed in the bath with respect to an Ag/AgCl pellet. Junction potentials were then measured in each solution with respect to the bath: −0.1 mV for Na^+, −2.8 mV for NH_4^+, and −3.5 mV for Cs^+.

Absolute membrane potentials were relevant only for the dependence of E_{REV} on K^+ (Fig. 1 *C*). Both measured and corrected values are shown for that experiment. Elsewhere, voltages shown are not corrected. Permeability ratios, calculated from shifts in E_{REV} using the flow tubes, were corrected for junction potential differences between test and control solutions, but did not need to be corrected for the initial electrode-bath junction.

RESULTS

The main protocols used to examine permeation for I_M and I_{DR} channels are illustrated in Fig. 1, *A* and *B*. I_M tail currents were observed on repolarization from the holding potential of −30 mV (Fig. 1 *A*). I_M is the time-dependent relaxation that develops as the channels close (Adams et al., 1982*a*). In this and other figures, I_M amplitude is the difference between the instantaneous current, measured just after the voltage change (5 to 10 ms) and the steady state current, measured at the end of the step (last 100 ms of a 1-s step). I_{DR} was activated by a step to +10 mV from a holding potential of −60 mV, and tail currents were then evoked at different voltages (Fig. 1 *B*). I_{DR} amplitude was simply the instan-

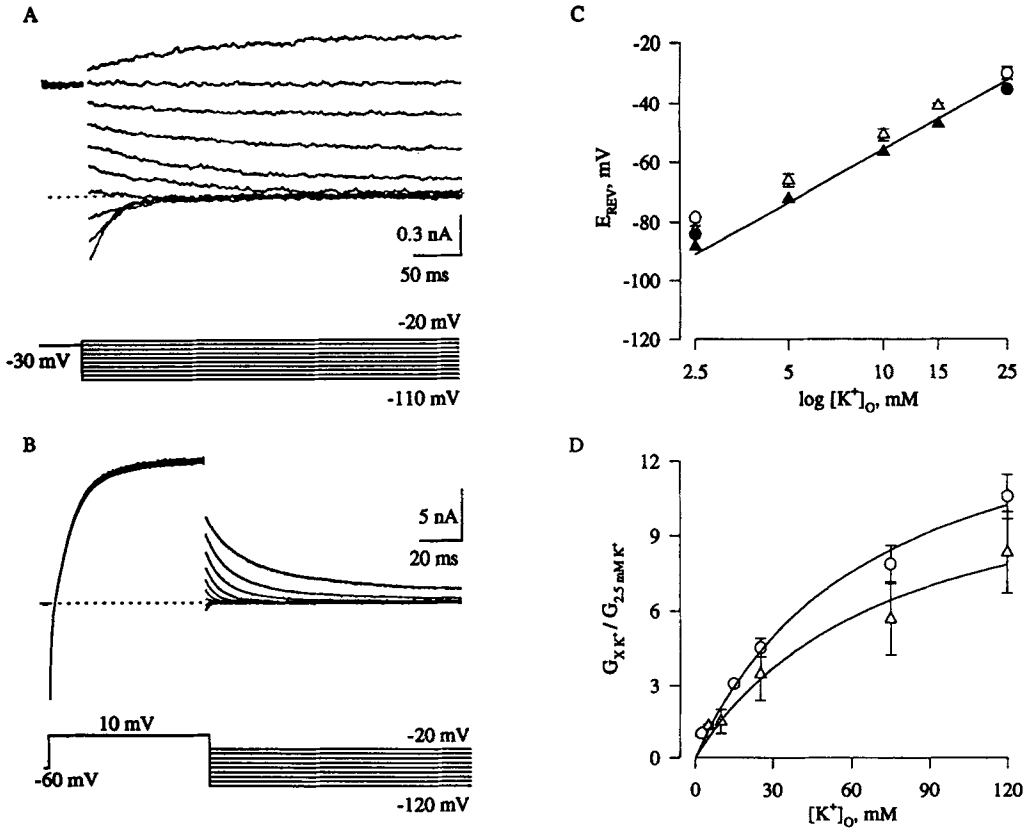

FIGURE 1. Sample records of I_M and I_{DR} in 2.5 mM K_o^+ plus 117.5 Na_o^+. (*A*) Superimposed I_M tail currents, recorded during 1-s steps to voltages between −20 and −110 mV, from a holding potential of −30 mV. Records from cell D4929, leak-subtracted (method 2; see Materials and Methods). In this and subsequent figures, zero current is denoted by a dotted line. (*B*) Superimposed I_{DR} traces. The standard protocol was to activate I_{DR} with a 75–90-ms step to +10 mV from a holding potential of −60 mV, and then repolarize to evoke tail currents. Leak-subtracted records from cell A4510. (*C*) Reversal potential (E_{REV}) plotted versus $[K^+]_o$ for I_M (*triangles*) and I_{DR} (*circles*). Increases in $[K^+]_o$ were compensated by decreases in $[Na^+]_o$. The solid symbols are E_{REV} after correction for junction potentials (see Methods). The line is the Nernst prediction for a K^+ electrode. (*D*) Conductance–$[K^+]_o$ relations for I_M (*triangles*) and I_{DR} (*circles*). For I_{DR}, NMG_o^+ replaced Na_o^+ in *D*. The lines are Michalis–Menten binding curves with appropriate K_M. Chord conductances were calculated from inward currents 30 mV negative to E_{REV} for each $[K^+]_o$, since E_{REV} varied with $[K^+]_o$. Conductances were normalized to the value at 2.5 mM K^+ in each cell.

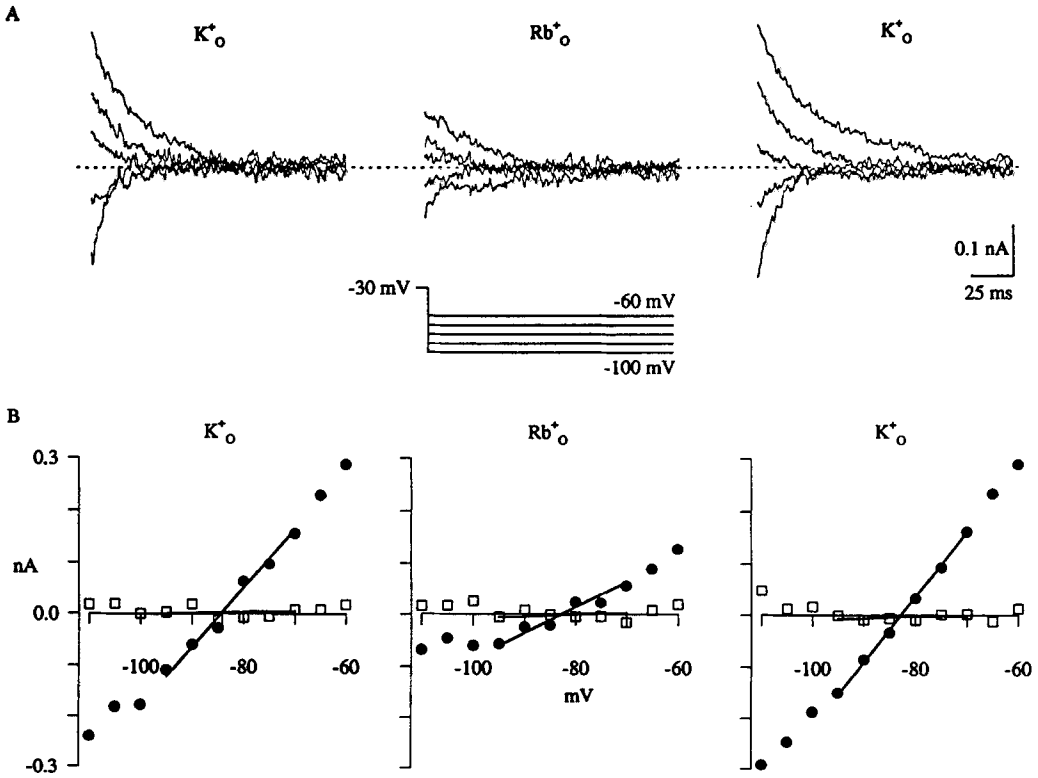

FIGURE 2. I_M in 2.5 mM K^+_o or Rb^+_o, plus 117.5 Na^+_o. (*A*) I_M tail currents in 2.5 mM K^+_o (*left*), 2.5 mM Rb^+_o (*middle*), and after return to K^+_o (*right*). The protocol was as in Fig. 1 *A*, but only the tail currents are shown here. Cell A4902, leak-subtracted (method 2). (*B*) *I–V* relations, from the data of *A*. Data were from 2.5 mM K^+_o, 2.5 mM Rb^+_o, and recovery in K^+_o (*left to right*). Instantaneous (*circles*) and steady-state (*squares*) currents were measured at the beginning and end of each tail current respectively. In this voltage region, there is little steady-state I_M. The straight lines are linear fits to the instantaneous and steady-state currents near E_{REV}. E_{REV} was estimated as the intersection of the lines, where the amplitude of the I_M relaxation would be zero.

taneous tail current (0.5–1 ms into the voltage step). Note that I_{DR} was considerably larger and faster than I_M. In physiologic ionic conditions (117.5 mM $[Na^+]_o$ and 2.5 mM $[K^+]_o$, 88 mM $[K^+]_i$), the equilibrium potential for K^+ (E_K) was −91.2 mV. The measured E_{REV} was −88.7 ± 1.5 mV (n = 28) for I_M and −84.4 ± 0.5 mV (n = 8) for I_{DR}, following correction for junction potentials (see Methods). The dependence of E_{REV} on $[K^+]_o$ was essentially as expected from the Nernst equation for a K^+ electrode (Fig. 1 *C*, *line*), indicating both channels were strongly selective for K^+ over Na^+ (discussed further below).

Ion channel conductance often saturates as a function of permeant ion concentration. Chord conductances for inward current were measured as a function of $[K^+]_o$. Fig. 1 *D* shows that the chord conductances could be fit by the Michalis–Menten equation with apparent K_M = 65 mM for I_{DR} and 71 mM for I_M. These values should not be taken literally as measures of the affinity of a binding site in the channel pore, for two reasons. First, a K_M measurement is not strictly valid in the case of a multi-ion pore, as there are two or more sites, each with its own binding affinity. Second, although the measured conductances primarily reflect ion influx, there is some contribution of efflux (see Methods). Thus, we present conductance values primarily as an empirical description.

K^+–Rb^+ Selectivity

Ion selectivity for I_M and I_{DR} channels was assessed by measuring both relative permeability and conductance for different extracellular ions. Fig. 2 shows the effects on I_M of equimolar replacement of 2.5 mM extracellular K^+ with Rb^+. Tail current amplitudes were clearly reduced in Rb^+_o, indicating a decreased conductance. E_{REV} for I_M was measured as the intersection between the instantaneous and steady-state currents after leak subtraction. There was no significant change in E_{REV}, indicating a permeability ratio (P_{Rb}/P_K) near 1.0 (Table I). Fig. 3 shows that P_{Rb}/P_K was also near 1.0 for I_{DR}, but G_{Rb} was only slightly less than G_K (Table I).

Because multi-ion pores may display concentration-dependent selectivity, P_{Rb}/P_K and G_{Rb}/G_K were also measured at higher $[K^+]_o$ and $[Rb^+]_o$. I_M was considerably reduced in 15 mM Rb^+_o, compared with 15 mM K^+_o

TABLE I

Relative Permeabilities and Conductances for I_M and I_{DR} Channels

Ion	I_M		I_{DR}	
	P_X/P_K	G_X/G_K	P_X/P_K	G_X/G_K
2.5 mM Rb_o^+	1.06 ± 0.04	0.42 ± 0.03	1.04 ± 0.01	0.77 ± 0.01
	(n = 14)	(n = 10)*	(n = 5)*	(n = 5)*‡
15 mM Rb_o^+	0.94 ± 0.03	0.35 ± 0.01	0.99 ± 0.01	0.87 ± 0.01
	(n = 13)	(n = 12)*	(n = 16)†	(n = 16)*†
25 mM Rb_o^+	—	—	0.97 ± 0.01	0.94 ± 0.01
			(n = 5)*‡	(n = 5)*‡
120 mM NH_{4o}^+	0.110 ± 0.004	0.32 ± 0.07	0.135 ± 0.004	0.93 ± 0.10
	(n = 5)	(n = 5)	(n = 5)	(n = 5)
120 mM Cs_o^+	0.10 ± 0.01	0.035 ± 0.004	0.099 ± 0.004	0.23 ± 0.01
	(n = 5)	(n = 5)	(n = 5)	(n = 5)
120 mM Na_o^+	< 0.004	—	0.0093 ± 0.0002	0.063 ± 0.008
	(n = 7)		(n = 17)	(n = 10)
120 mM Li_o^+	< 0.004	—	< 0.004	—
	(n = 7)		(n = 7)	
120 mM $CH_3NH_{3o}^+$	< 0.004	—	< 0.004	—
	(n = 7)		(n = 7)	

For K_o^+ and Rb_o^+, P_{Rb}/P_K and G_{Rb}/G_K were compared at the same concentration. For NH_{4o}^+, Cs_o^+, and Na_o^+, P_X/P_K and G_X/G_K were calculated by comparison to data at 2.5 mM K_o^+. To calculate G_X/G_K for NH_4^+, Cs^+, and Na^+, G_K at 120 mM K_o^+ was estimated by multiplying the measured G_K at 2.5 mM K_o^+ by 8.34 for I_M or 10.56 for I_{DR} (the average $G_{120\text{ mM K}}/G_{2.5\text{ mM K}}$ from Fig. 1*D*). For I_M, E_{REV} with NH_{4o}^+ was measured using the protocol of Fig. 4 *C*. Where noted, Rb^+/K^+ ratios were significantly different * from 1.0,† from the value at 2.5 mM K_o^+, or ‡ from the value at 15 mM K_o^+.

(Fig. 4, *A* and *B*). The reversal potential was near −30 mV in 15 mM K_o^+, where I_M was almost completely activated (see Fig. 6). Thus I_M relaxations were small near E_{REV} as few I_M channels closed. To better resolve E_{REV}, a different voltage protocol was used. First, most I_M channels were closed by a 350 ms prepulse to −80 mV from the holding potential of −30 mV, and I_M was then observed to activate on depolarization from −80 mV (Fig. 4 *C*). As before, I_M amplitude was the difference between instantaneous and steady-state currents, and E_{REV} was the point of zero relaxation, i.e., a flat trace. For I_M, P_{Rb}/P_K and G_{Rb}/G_K did not change significantly be-

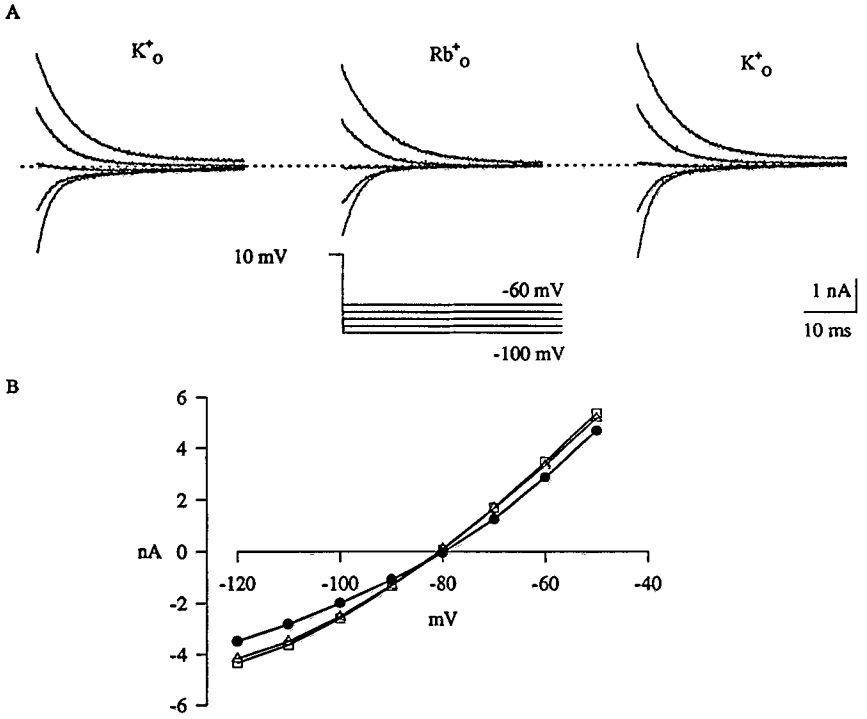

FIGURE 3. I_{DR} in 2.5 mM K_o^+ or Rb_o^+, plus 117.5 mM NMG_o^+. (*A*) I_{DR} tail currents in 2.5 mM K_o^+ (*left*), 2.5 mM Rb_o^+ (*middle*), and at complete recovery in K_o^+ (*right*). E_{REV} was measured as the point of zero instantaneous current. (*B*) Instantaneous *I–V* relations, from the experiment of part *A*. Open symbols are currents measured in K_o^+, and filled circles in Rb_o^+. Cell F4O14.

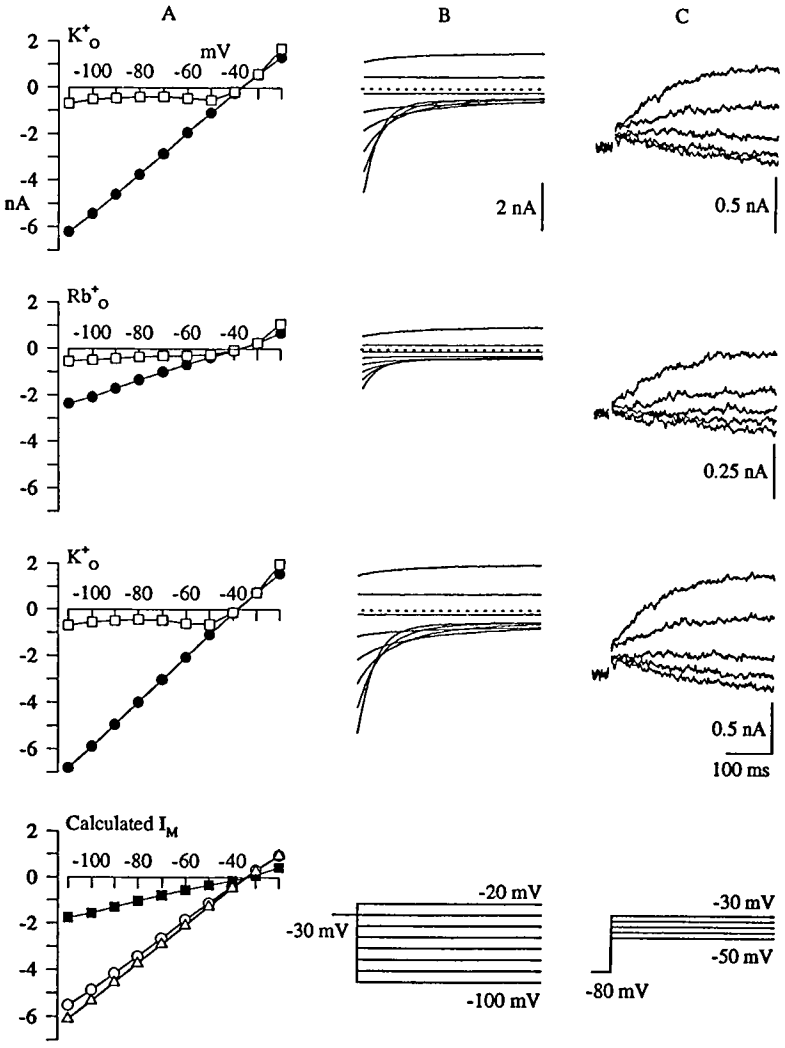

FIGURE 4. I_M in 15 mM K^+_o or Rb^+_o, plus 117.5 Na^+_o. (*A*) *I–V* relations for instantaneous (*circles*) and steady state (*squares*) tail currents, in 15 mM K^+_o, 15 mM Rb^+_o, and return to K^+_o (from top downward). These measurements are not leak-subtracted. The calculated I_M after linear leak subtraction (method 1) is shown in the bottom panel, with open symbols in K^+_o and filled symbols in Rb^+_o. (*B*) The I_M tail currents that were measured in part *A*, not leak-subtracted. (*C*) I_M activated by depolarizing steps from −80 mV, using the voltage protocol illustrated at the bottom. Records were leak-subtracted. I_M is the time-dependent current during the −30 to −50 mV steps. The instantaneous outward current at the beginning of each step reflects I_M that was not deactivated by the 350-ms period at −80 mV. Data are from cell B4N03.

tween 2.5 and 15 mM (Table I). It was not possible to accurately measure P_{Rb}/P_K or G_{Rb}/G_K for I_M channels at higher concentrations of K^+_o or Rb^+_o, as E_{REV} was at depolarized voltages where I_M was not well isolated from I_{DR}.

I_{DR} tails were also measured in 15 mM K^+_o versus 15 mM Rb^+_o, and at 25 mM (Table I). There was little change in reversal potential ($P_{Rb}/P_K \sim 1$), but a detectable decrease in the amplitude of inward currents in Rb^+_o. For I_{DR}, there were statistically significant differences in G_{Rb}/G_K with concentration (Table I), which is a sign of multi-ion pore behavior.

Multi-ion pores often show an anomalous mole fraction effect. This was examined by recording currents in mixtures of K^+_o and Rb^+_o, at a total concentration of 15 mM. E_{REV} (permeability) and chord conductance were determined as for 15 mM K^+_o. For I_{DR}, but not I_M, channel permeability was slightly reduced in the mixtures, compared with Rb^+_o or K^+_o alone (Fig. 5). The permeabilities in 66% and 33% K^+_o were significantly less than the values in pure Rb^+_o or pure K^+_o (Fig. 5 *B*) ($P<0.001$, paired two-tailed t tests). The effect was small, but a multi-ion pore can show a strong anomalous mole fraction effect, a weak one, or none at all, depending on the energy profiles and the ion concentrations (Campbell et al., 1988).

R. Cloues and N. V. Marrion (personal communication) also found no significant anomalous mole fraction effect for I_M in rat sympathetic ganglia, using isotonic K^+_o + Rb^+_o. Our attempts to reproduce their result were complicated by large I_{SA}-like currents (Selyanko et al., 1990), which were much more prominent in 120 mM Rb^+_o than in K^+_o or in our previously used ionic conditions (see Materials and Methods). However, we could identify a tail current component with I_M-like kinetics, which showed no anomalous mole fraction effect in mixtures of 120 mM K^+_o + Rb^+_o (data not shown).

Interpretation of Conductance Measurements

The amplitude of a whole-cell current reflects both the single-channel current and the number of open channels. Thus, if activation of I_M or I_{DR} changed when Rb^+_o

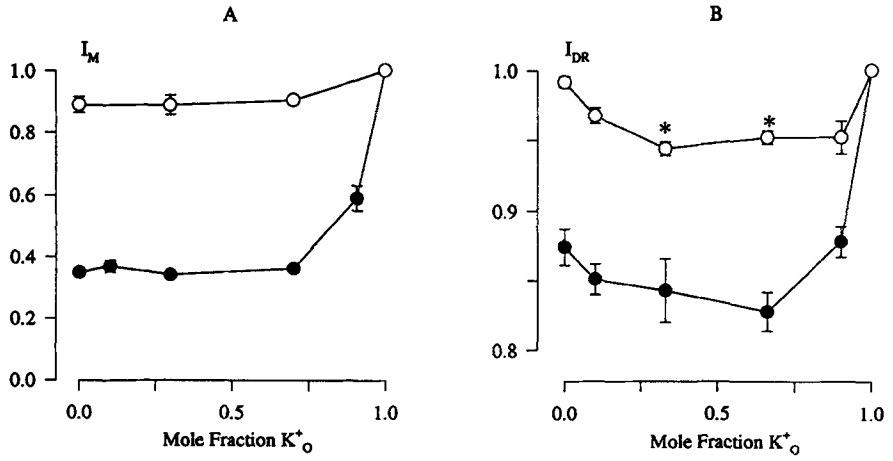

FIGURE 5. Test for anomalous mole fraction effects. $[K^+]_o + [Rb^+]_o$ was held constant at 15 mM, with the mole fraction of K_o^+ varied from 0.0 (pure Rb_o^+) to 1.0 (pure K_o^+). Conductances (*filled circles*) and permeabilities (*open circles*) are shown for I_M (*A*) in 105 mM Na_o^+ and I_{DR} (*B*) in 105 mM NMG_o^+. Note expanded vertical scale in *B*. Error bars are shown when larger than the symbols. Asterisks denote values that were significantly less than those at K_o^+ mole fractions of 0.0 and 1.0.

was substituted for K_o^+, the differences in the measured chord conductances might reflect changes in gating rather than permeation. Therefore, the voltage dependence of activation was measured for both currents in the different ionic conditions, using tail currents recorded at a fixed voltage (−60 mV) to assess the degree of activation during preceding voltage steps.

After depolarizations lasting 1 s, from a holding potential of −30 mV, tail currents contained both fast I_{DR} and slow I_M components (Fig. 6, *A* and *C*). The I_M component was fitted to a Boltzmann relation (Fig. 6, *B* and *D*), as in the original kinetic description of I_M (Adams et al., 1982*a*). Table II shows that I_M activation parameters did not vary significantly between K_o^+ and Rb_o^+. The Boltzmann parameters were comparable with those of Adams et al. (1982*a*), except for a ~10 mV hyperpolarized shift in $V_{1/2}$, probably resulting from differences in screening of surface charge by the different

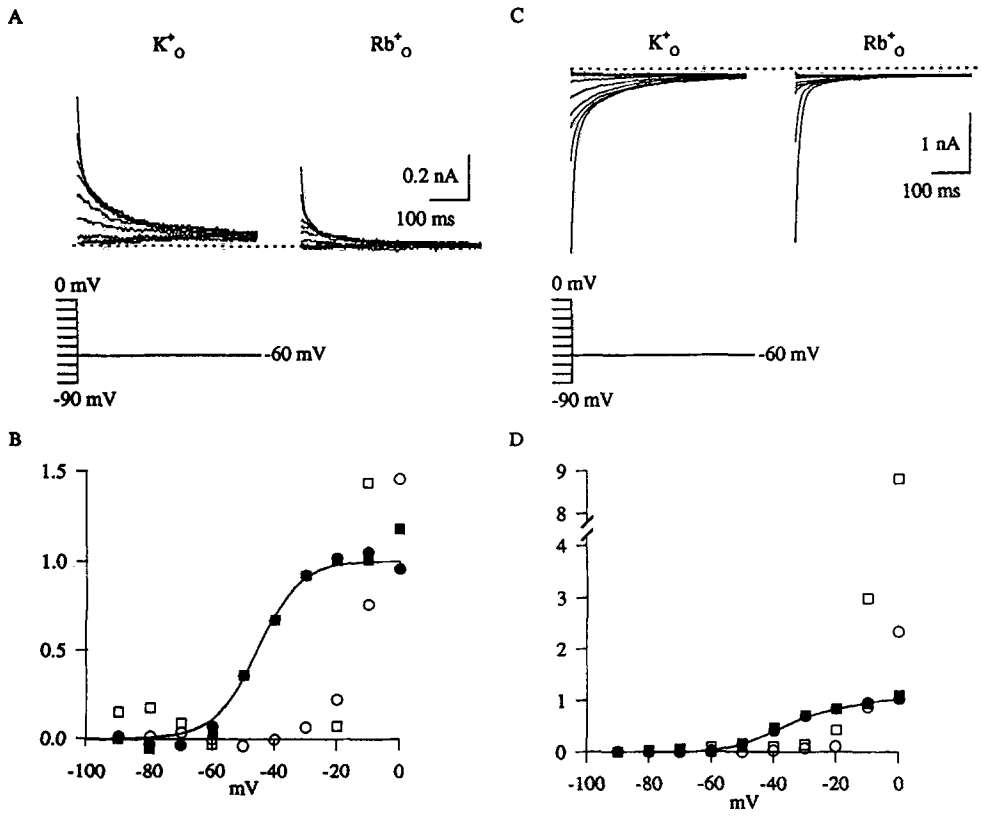

FIGURE 6. Comparison of I_M activation curves in K_o^+ vs. Rb_o^+. $[K^+]_o$ or $[Rb^+]_o$ was 2.5 mM for *A* and *B*, and 15 mM for *C* and *D*. (*A*) Tail currents at −60 mV in 2.5 mM K_o^+ (*left*) or 2.5 mM Rb_o^+ (*right*), after 1-s steps to the voltages indicated below the traces. Records are not leak-subtracted. Cell E4902. (*B*) I_M activation curves (*filled symbols*). *Circles* denote measurements in K_o^+, *squares* in Rb_o^+. For comparison, the I_{DR} tail component is also shown (*open symbols*). The line is the Boltzmann fit to the I_M data in K_o^+, with $V_{1/2} = -46$ mV and $z = 3.6$. I_M tails were separated from I_{DR}, and data were fitted to the Boltzmann relation (Eq. 3), as described in Methods. The activation curve was scaled such that $I_{M,max} = 1$ and $I_{M,0} = 0$ (see Eq. 3). I_{DR} tails were normalized to $I_{M,max}$, to allow comparison of I_M and I_{DR} amplitudes. (*C*) Tail currents in 15 mM K_o^+ (*left*) or Rb_o^+ (*right*) at −60 mV, as in part *A*. Cell A5123. (*D*) Normalized activation curve from the data of *C*. The data were analyzed, and symbols have the same meaning, as in *B*. Note that the value for I_{DR} at 0 mV in Rb_o^+ (8.8) is off scale. The line is the Boltzmann fit to the I_M data in K_o^+, with $V_{1/2} = -36$ mV and $z = 3.1$.

TABLE II

Activation Parameters for I_M and I_{DR} in Different Ionic Conditions

	I_M			I_{DR}		
Ion	z	$V_{1/2}$ (mV)	n	z	$V_{1/2}$ (mV)	n
2.5 mM K_o^+	3.6 ± 0.3	−46.9 ± 3.5	5	1.7 ± 0.04	10.0 ± 3.1	6
2.5 mM Rb_o^+	4.0 ± 0.5	−45.4 ± 3.7	5	1.9 ± 0.1	8.8 ± 3.9	4
15 mM K_o^+	2.9 ± 0.5	−34.3 ± 7.6	5	1.7 ± 0.1	2.0 ± 2.1	6
15 mM Rb_o^+	2.8 ± 0.1	−38.2 ± 1.4	5	1.8 ± 0.1	2.8 ± 3.9	4

I_M tail currents were separated from I_{DR}, and data were fitted to the Boltzmann relation (Eq. 3), as described in Materials and Methods.

divalent ion concentrations used (10 mM Mg^{2+}_o + 2 mM Ca^{2+}_o for Adams et al., 1982*a*; vs. 2 mM Mn^{2+}_o in the experiments reported here).

I_{DR} activation was measured with a separate protocol, using depolarizations from a holding potential of −60 mV. This required attenuating the outward current, because it was too large to clamp accurately with 88 mM intracellular K^+. Two methods were used. First, 2 mM TEA_o was added to partially block I_{DR}. TEA block did not affect E_{REV} in 2.5 or 15 mM K_o^+ or Rb_o^+ ($n = 5$), and does not change the activation curve of I_{DR} (K.J. Greene and S.W. Jones, unpublished observation). Tail current amplitudes were fitted to a Boltzmann relation to provide an empirical comparison between cells and ionic conditions. Although high Rb_o^+ and K_o^+ both slowed tail current deactivation, the I_{DR} activation curves did not vary between K_o^+ and Rb_o^+ (Table II). I_{DR} activation was also measured without TEA, but with a lower K^+ intracellular solution (25 mM), and again, activation did not vary between Rb_o^+ and K_o^+ (data not shown). Thus, for both I_M and I_{DR}, differences in chord conductance between K_o^+ and Rb_o^+ are likely to reflect differences in permeation, not gating.

Other Monovalent Cations

Both currents were tested in a variety of external cations. As expected from other K^+ channels (Hille, 1992), both I_M and I_{DR} channels were weakly permeable to 120 mM NH_{4o}^+, but not measurably permeable to Li_o^+, $CH_3NH_{3o}^+$, or NMG_o^+ (Fig. 7, Table I). No inward current was observed as far negative as −120 mV when the sole extracellular monovalent cation was 120 mM Li^+, $CH_3NH_3^+$, or NMG^+.

Cs_o^+ could carry inward current for both I_M and I_{DR} (Fig. 7). The relative permeabilities and chord conductances were small but measurable (Table I). Unexpectedly, I_{DR} channels were also permeable to Na_o^+ (Fig. 7, Table I). Because of the extremely negative reversal (<−100 mV) in 120 mM Na_o^+, the chord conductance could only be measured 10–20 mV negative to reversal. Therefore, the value for Na^+ conductance in Table I

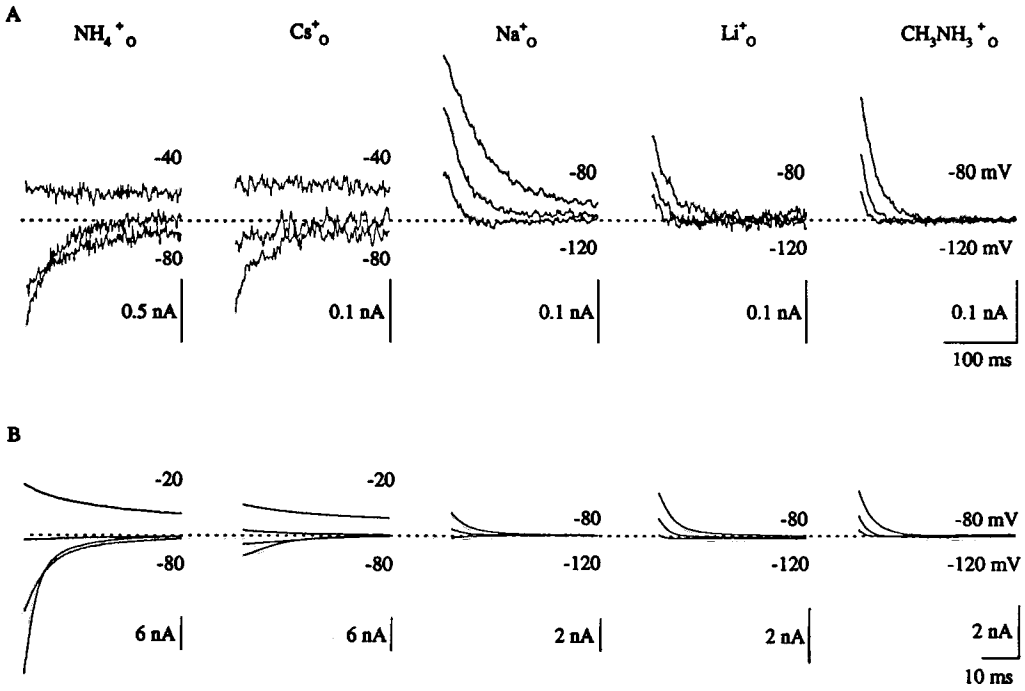

FIGURE 7. I_M and I_{DR} in 120 mM extracellular NH_4^+, Cs^+, Na^+, Li^+, or $CH_3NH_3^+$. Tail currents are shown in 20 mV increments for I_M (*A*) and I_{DR} (*B*). The voltage range for the tail currents is given adjacent to the current traces. Note the different current scales. I_M records were taken from different cells (NH_4^+, A4920; Cs^+, A4921; Na^+, F4902; Li^+, A4920; $CH_3NH_3^+$, A4920) and were leak subtracted ("method 2"). All I_{DR} records are from cell C4921.

may overestimate the true Na^+ conductance through I_{DR} channels, but that value was clearly greater than zero. In contrast to I_{DR}, I_M channels did not conduct a measurable Na^+ current (Fig. 7).

Because detectable Na^+ and Cs^+ permeability through K^+ channels is not generally observed, we attempted to rule out several possible artifactual explanations for this result. Inward Cs^+ and Na^+ currents were not an artifact of the leak subtraction method, as they were observed in both leak-subtracted and unsubtracted records (data not shown). There were no other permeant ions in the extracellular solution, leaving Na^+ or Cs^+ as the only possible carrier of inward current. Inward Na^+ and Cs^+ currents were especially obvious when compared with current traces with Li^+, $CH_3NH_3^+$, or NMG^+ as the sole extracellular monovalent cations (Fig. 7). The lack of inward current with Li_o^+, $CH_3NH_{3o}^+$, or NMG_o^+ also ruled out the possibility that the inward current observed with Na_o^+ or Cs_o^+ was actually the result of accumulation of extracellular K^+ during the preceding depolarizing step. Additionally, I_{DR} Na^+ current was also observed under conditions that minimized any possible K^+ accumulation, shortening the depolarizing step to 30 ms or stepping to only −10 mV (data not shown). Another conceivable possibility was that the Na^+-K^+ ATPase might be active in 120 mM extracellular Na^+, but not NMG^+, Li^+, or $CH_3NH_3^+$, which could affect ion gradients. To test that possibility, the 120 mM Na^+ experiments were repeated with the Na^+-K^+ ATPase inhibited by 100 μM dihydroouabain (Jones, 1989). As before, inward Na^+ current through I_{DR} channels was observed (data not shown). Finally, K^+ contamination of the NaCl used was minimal, <0.005% K^+ (SigmaUltra grade), predicting at most 6 μM K^+ and an $E_K = -245$ mV.

Ion Block

I_{DR} channels were permeable to Na^+ but only carried a small Na^+ current. If Na_o^+ truly entered the pore, it might block K^+ current through I_{DR} channels. Extracellular Na^+, at 25 and 100 mM, did block inward K^+ current through I_{DR} channels in a voltage-dependent manner, with 10 mM K_o^+ (Fig. 8). A Woodhull (1973) scheme was used to quantify the block in terms of intrinsic binding affinity ($K_{D(0\ mV)}$) and effective valence ($z\delta$):

$$f = [X^+]_o / \{ [X^+]_o + K_{D(0\ mV)} \exp(z\delta FVR^{-1}T^{-1}) \}, \quad (4)$$

where f = the fraction of I_{DR} tail currents blocked by ion X^+ at the voltage V. That simplified version of the Woodhull (1973) model is not strictly valid here, as it assumes that the blocking ion binds at a fixed electrical distance (δ) from the extracellular space without permeating the channel, and it does not consider ion–ion interactions in the pore. Current block was not well described by a single set of parameters for both Na_o^+ concentrations (Fig. 8, *dashed lines*). However, each Na_o^+

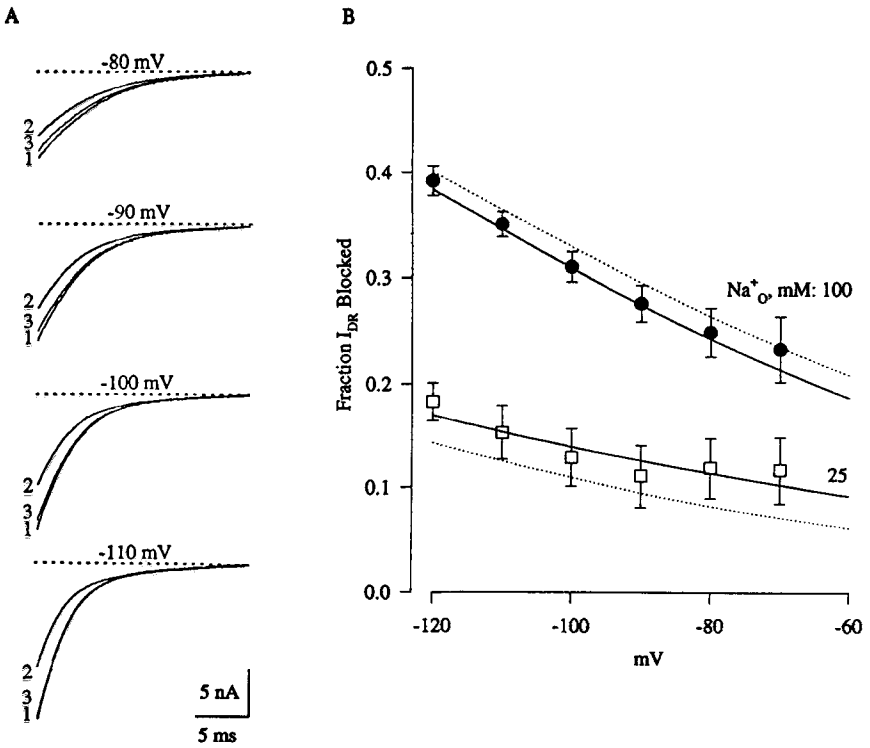

FIGURE 8. Extracellular Na^+ block of inward K^+ current through I_{DR}. (*A*) I_{DR} tail currents in 10 mM K_o^+ + 100 mM NMG_o^+ (*1*), 10 mM K_o^+ + 100 mM Na_o^+ (*2*), and after return to 10 mM K_o^+ + 100 mM NMG_o^+ (*3*), recorded at the voltages indicated after repolarization from +10 mV. Cell A4N02. (*B*) Woodhull (1973) plot of the fraction of I_{DR} blocked vs. voltage, for 25 mM Na_o^+ (*squares*) and 100 mM Na_o^+ (*circles*). Dotted curves are the best fit of Eq. 4 to data in both 25 and 100 mM Na_o^+, with $K_{D(0\ mV)}$ = 967 mM, $z\delta = 0.40$ ($n = 6$). Solid curves are fits to each Na_o^+ concentration individually: $K_{D(0\ mV)}$ = 496 mM and $z\delta = 0.30$ for 25 mM Na_o^+; $K_{D(0\ mV)}$ = 1.18 M and $z\delta = 0.43$ for 100 mM Na_o^+.

concentration could be well fit individually (*solid lines*). Concentration dependence of effective valence has been interpreted previously as evidence of multi-ion pore behavior (Adelman and French, 1978). Na_o^+ did not block inward I_M under the same ionic conditions (data not shown).

The block of inward I_{DR} by Na_o^+, observed in high K_o^+, suggested that Na_o^+ might affect I_{DR} under physiologic conditions (see Fig. 1 *B*). Figure 9 shows that Na_o^+ also blocked I_{DR} in 2.5 mM K_o^+. Furthermore, the outward rectification in the instantaneous I–V curve was markedly increased in Na_o^+ compared with NMG_o^+ ($n = 4$). Na^+ permeation in I_{DR} channels might affect E_{REV}, as suggested by the observation that E_{REV} was slightly positive to the calculated E_K in 2.5 mM K_o^+ (Fig. 1 *C*). The Goldman-Hodgkin-Katz (GHK) equation predicts a shift of +9 mV on switching from NMG_o^+ to Na_o^+, for $P_{Na}/P_K = 0.009$ and $P_{NMG}/P_K = 0$. However, no significant shift was observed (-1.6 ± 0.5 mV, $n = 4$). The GHK equation assumes that permeant ions do not interact, which is not true in a multi-ion pore. The absence of an E_{REV} shift with Na_o^+ suggests that the I_{DR} channel pore does not obey independence between K^+ and Na^+, which is additional evidence that I_{DR} channels are multi-ion pores.

As Cs^+ was also both permeant and weakly conducting, extracellular Cs^+ block of both currents was tested. Both I_M and I_{DR} were blocked by Cs_o^+ in a strongly voltage-dependent manner. Cs_o^+ block of I_M at all three Cs_o^+ concentrations was well fit by a single set of Woodhull parameters (Fig. 10). Similarly to Na_o^+, Cs_o^+ block of I_{DR} was not fit well by a single set of parameters for the entire data set (Fig. 11, *dashed lines*), but each Cs_o^+ concentration was well fit individually (Fig. 11, *solid lines*). The best fit effective valence did not change monotonically with Cs^+ ($z\delta = 0.63$ in 1 mM Cs_o^+, 0.96 in 25 mM Cs_o^+, and 0.70 in 75 mM Cs_o^+).

Eyring Models of Permeation

A two-barrier one-site model could fit I_M adequately in K_o^+, Rb_o^+, and Cs_o^+ (Fig. 12). The barriers and wells were fixed to be at the same electrical locations for all three ions, and the same set of parameters was used for both Cs_o^+ block and Cs_o^+ permeation. In contrast, the K_o^+-Rb_o^+ data for I_{DR} required a three-barrier two-site model, and block of I_{DR} by Cs_o^+ could not be adequately described even by the two-site model (not shown).

DISCUSSION

I_{DR}

In many ways, permeation properties of I_{DR} channels in bullfrog sympathetic neurons were similar to many

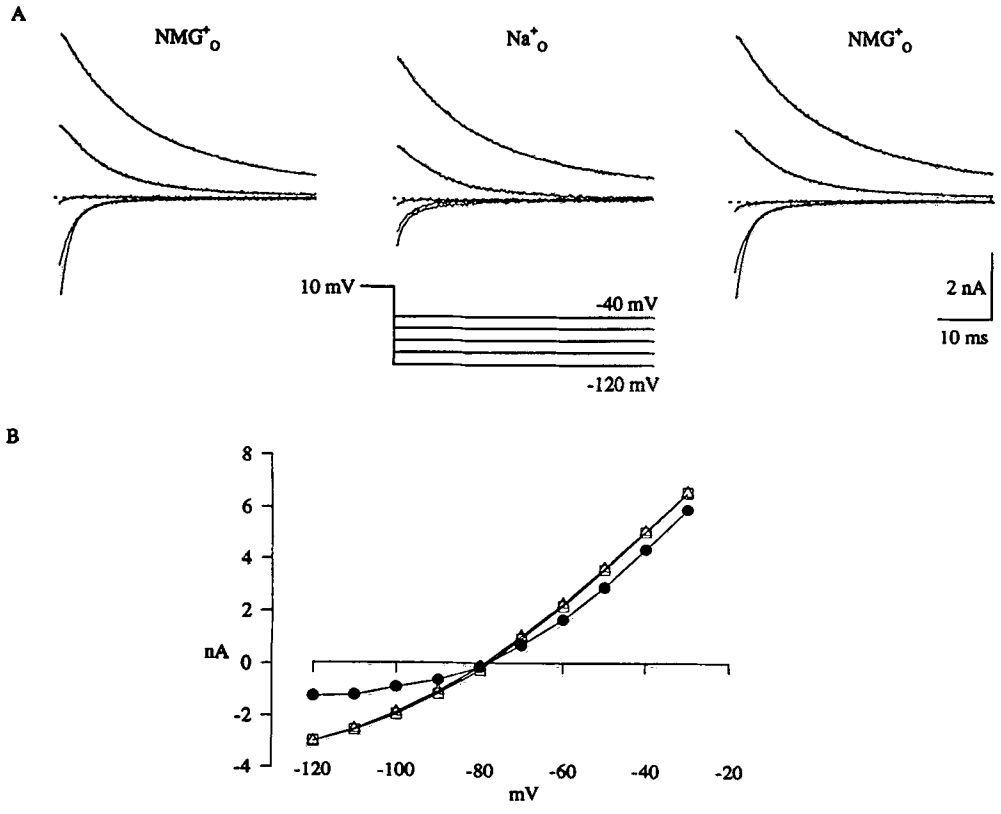

FIGURE 9. Na_o^+ block of I_{DR} under physiological conditions. Because there was a large junction potential difference between Na_o^+ and NMG_o^+ solutions, a 3-M KCl agar bridge was used as bath ground in these experiments, and solutions were exchanged by bath. (*A*) I_{DR} tail currents in 2.5 mM K_o^+ + 117.5 mM NMG_o^+ (*left*), K_o^+ + 117.5 mM Na_o^+ (*middle*), and after return to K_o^+ + NMG_o^+ (*right*). (*B*) Instantaneous *I–V* relations from the data in part *A*. Open symbols are currents measured in NMG_o^+, filled symbols in Na_o^+. Cell A5517.

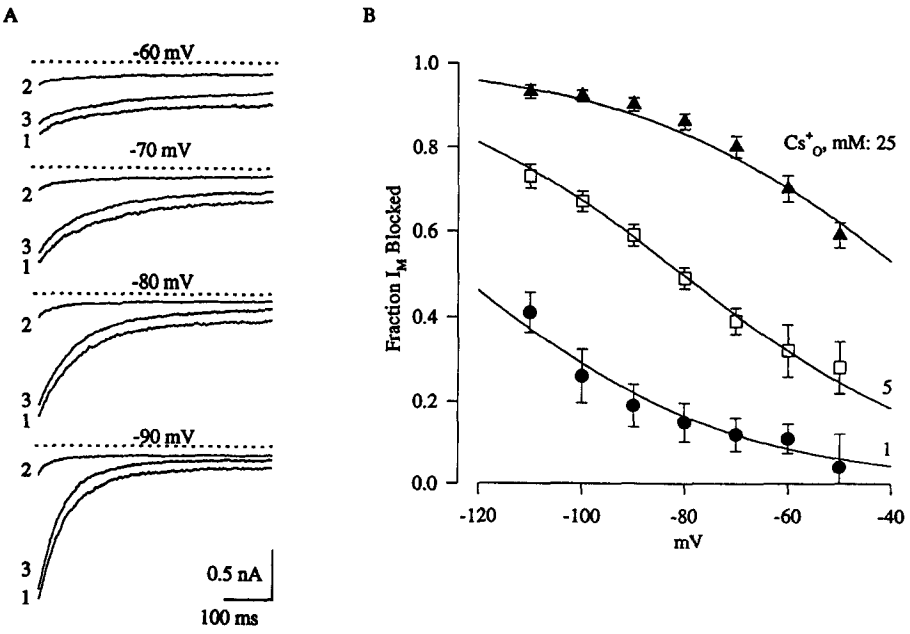

FIGURE 10. Extracellular Cs^+ block of inward I_M. (*A*) I_M tail currents in 25 mM K^+_o (*1*), 5 mM Cs^+_o + 25 mM K^+_o (*2*), and after return to 25 mM K^+_o (*3*), at the indicated voltages, all with Na^+_o to balance ionic strength. Currents are not leak-subtracted. The apparent decrease in current between initial and final measurements was the result of a small decrease in leak, which did not affect the amplitude of the I_M relaxation. Cell A3O28. (*B*) The fraction of I_M blocked by Cs^+_o vs. voltage, in 25 mM $[K^+]_o$. $[Cs^+]_o$ was 1 mM (*circles*), 5 mM (*squares*), or 25 mM (*triangles*). Curves are the best fit of Eq. 4 to the data, with $K_{D(0\ mV)}$ = 97 mM and $z\delta$ = 0.93 (n = 8).

other K^+ channels. Rb^+ permeability was comparable to frog node (P_{Rb}/P_K = 0.92, Hille, 1973) and *Shaker* (P_{Rb}/P_K = 0.89; Perez-Cornejo and Begenisich, 1994) K^+ channels. Perez-Cornejo and Begenisich (1994) also observed concentration dependence in P_{Rb}/P_K, while others have reported that G_{Rb}/G_K was lower than P_{Rb}/P_K (Wagoner and Oxford, 1987; Shapiro and DeCoursey, 1991; Heginbotham and MacKinnon, 1993). Anomalous mole fraction effects have been seen in many K^+ channels, including inward rectifier, Ca^{2+}-activated, squid axon, and *Shaker* K^+ channels (Hagiwara et al., 1977; Eisenman et al., 1986; Wagoner and Oxford, 1987; Heginbotham and MacKinnon, 1993). NH_4^+ permeability was also similar to previously reported data (Hille, 1973; Reuter and Stevens, 1980; Wagoner and Oxford, 1987; Shapiro and DeCoursey, 1991; Heginbotham and MacKinnon, 1993; Perez-Cornejo and Begenisich, 1994).

Na^+ Permeation and Block of I_{DR}

K^+ channels usually exclude Na^+ very effectively (Hille, 1992). The combination of observable Na^+ currents through I_{DR} channels (Fig. 7) and voltage-dependent

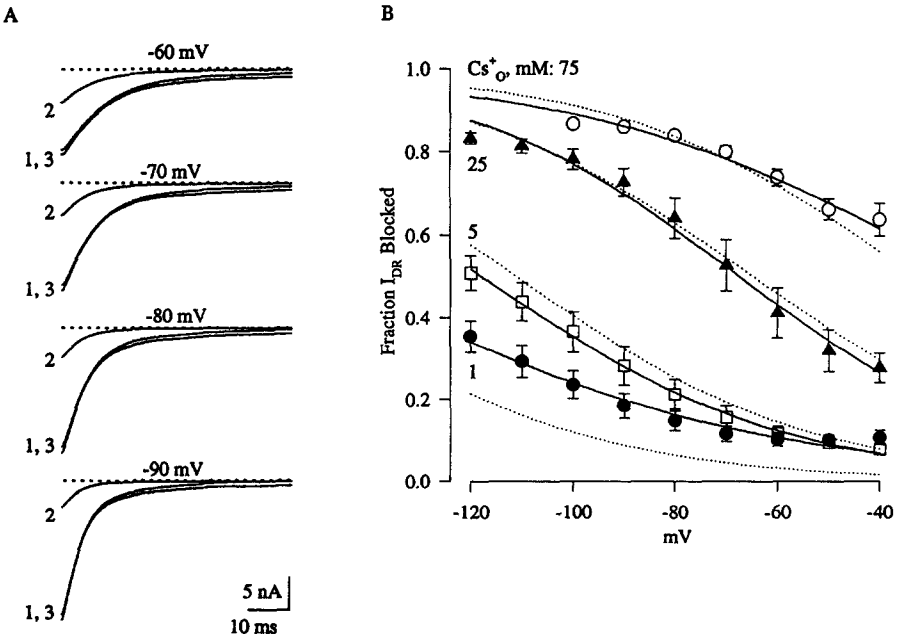

FIGURE 11. Extracellular Cs^+ block of inward I_{DR}. (*A*) I_{DR} tail currents in 25 mM K^+_o (*1*), 25 mM Cs^+_o + 25 mM K^+_o (*2*), and after return to 25 mM K^+_o (*3*), at the indicated voltages. All traces from cell E4O14 and with NMG^+_o to balance ionic strength. (*B*) The fraction of I_{DR} blocked by Cs^+_o vs. voltage, in 25 mM $[K^+]_o$. Dotted curves are the best fit of Eq. 4 to all four Cs^+_o concentrations, with $K_{D(0\ mV)}$ = 238 mM and $z\delta$ = 0.90 (n = 11). Solid curves are fits to each Cs^+_o concentration individually: $K_{D(0\ mV)}$ = 36 mM and $z\delta$ = 0.63 in 1 mM Cs^+_o (*filled circles*); $K_{D(0\ mV)}$ = 269 mM and $z\delta$ = 0.88 in 5 mM Cs^+_o (*squares*); $K_{D(0\ mV)}$ = 306 mM and $z\delta$ = 0.96 in 25 mM Cs^+_o (*triangles*); $K_{D(0\ mV)}$ = 139 mM and $z\delta$ = 0.70 in 75 mM Cs^+_o (*open circles*).

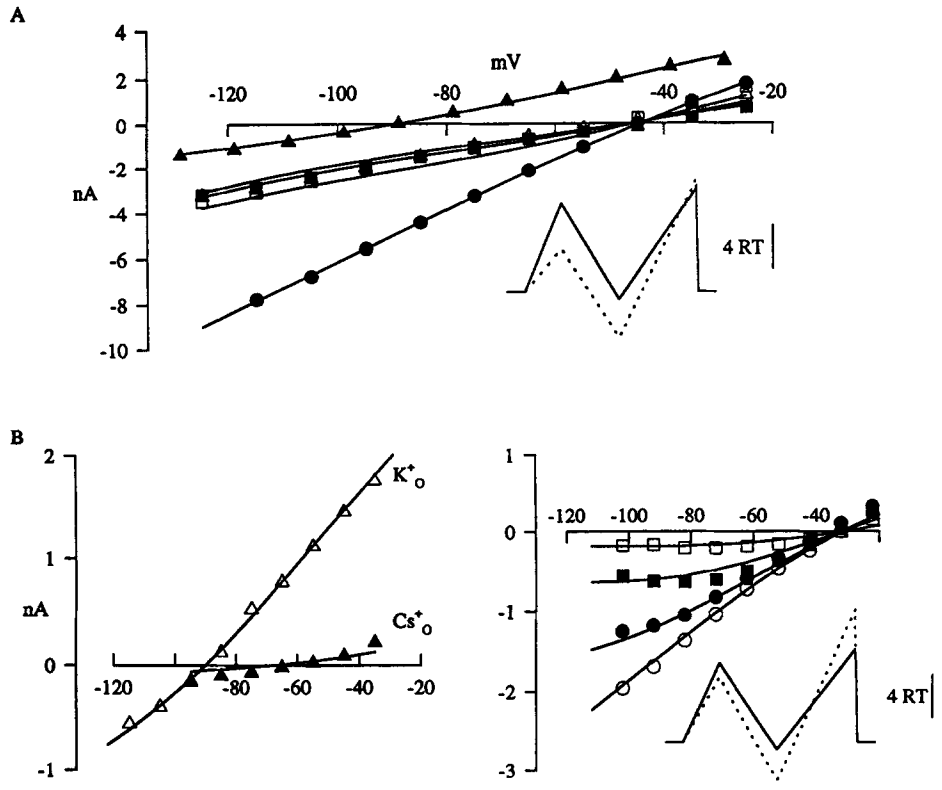

FIGURE 12. A two-barrier one-site Eyring model for I_M. Data are instantaneous currents from the protocol of Fig. 1 *A* (*symbols*), with the model superimposed (*curves*). Model currents were calculated from Eq. 14–10 of Hille (1992). Data were corrected for junction potentials. (*A*) I_M in K^+_o and Rb^+_o from cell B4N09, recorded in 2.5 mM K^+_o (*filled triangles*), 15 mM K^+_o (*filled circles*), 15 mM Rb^+_o (*filled squares*), 5 mM K^+_o + 10 mM Rb^+_o (*open squares*), and 10 mM K^+_o + 5 mM Rb^+_o (*open triangles*). The inset shows the energy profile, with barrier and well free energies (in RT units) 8.3, −0.7, 9.7 for K^+ (*solid lines*), and 4.0, −4.3, 10.5 for Rb^+ (*dashed lines*). The outer barrier was not uniquely defined for Rb^+, as the error in the fit changed little for values from 0 − 4 RT. The barrier heights given predict single-channel-sized currents (~pA). The simulated whole-cell currents in this figure were generated by arbitrarily assuming 1,000 channels per cell. Electrical distances were 0.21, 0.54, and 0.99 from outside to inside (*left to right*). (*B*) I_M in K^+_o and Cs^+_o. At the left, currents in 120 mM Cs^+_o with no K^+_o (*filled symbols*) and 2.5 mM K^+_o + 117.5 Na^+_o (*open symbols*), from cell A4921. At the right, Cs^+_o block of I_M in 25 mM K^+_o + Na^+_o (*open circles*), with 1 (*filled circles*), 5 (*filled squares*), or 25 (*open squares*) mM Cs^+_o added, from cell D3O28. The inset shows the energy profile, with barriers/wells 6.8, −4.0, and 13.7 for Cs^+ (*dashed lines*), and the same K^+ profile and electrical distances as in part *A*. The K^+ energy profile from part *A* was used to fit the K^+ data in *B*, adjusting only the number of channels per cell. The Cs^+ energy profile was derived by fitting the data for both Cs^+_o permeation and Cs^+_o block.

Na^+_o block of inward K^+ current (Figs. 8 and 9) was strong evidence that Na^+_o both entered and traversed the pore. In contrast, Na^+ was not measurably permeant in a variety of other K^+ channels, including I_M, frog node (Hille, 1973), inward rectifier (Hagiwara and Takahashi, 1974), Ca^{2+}-dependent K^+ (Blatz and Magleby, 1984; Tabcharani and Misler, 1989; Hu et al., 1989), *Shaker* (Heginbotham and MacKinnon, 1993), and Kv2.1 K^+ channels (Kirsch et al., 1995). Extracellular Na^+ had little effect on K^+ currents in the squid axon (Bezanilla and Armstrong, 1972; Adelman and French, 1978). However, internal Na^+ did block squid axon K^+ current, and the block was relieved by extreme depolarization, implying that Na^+ could traverse the pore, but at a low rate (French and Shoukimas, 1985). Ca^{2+}-dependent K^+ channels were also blocked asymmetrically by internal but not external Na^+ (Yellen, 1984). Those results contrast with the block by extracellular Na^+ reported here for the I_{DR} of frog sympathetic neurons. We are not aware of any previous evidence for block of K^+ channels by Na^+_o, which we observed even under physiologic ionic conditions (Fig. 9).

A few studies have reported detectable Na^+ currents through K^+ channels. Reuter and Stevens (1980) found P_{Na}/P_K = 0.07 for the delayed rectifier of *Helix* neurons. Taylor (1987) measured putative inward Na^+ currents for the *Helix* A-current, predicting P_{Na}/P_K = 0.09, but those results were complicated by possible K^+ accumulation. The *eag* K^+ channel of *Drosophila* showed an unusually high Na^+ permeability (P_{Na}/P_K = 0.11; Brüggemann et al., 1993), but the rat homolog of *eag* did not ($P_{Na}/P_K < 0.01$; Ludwig et al., 1994). Our ability to record a Na^+ current through I_{DR} channels was probably the result of the strong hyperpolarizing pulses used, which were necessary because Na^+ permeability was small. Many studies that did not find a measurable P_{Na}/P_K did not use such extreme voltages, and thus were only able to conclude that P_{Na}/P_K was <0.01, consistent with the P_{Na}/P_K = 0.009 reported here for I_{DR}.

Some K^+ channels become permeable to Na^+ under abnormal ionic conditions, including the absence of K^+ and/or Ca^{2+} (Armstrong and Miller, 1990; Zhu and Ikeda, 1993; Callahan and Korn, 1994; Korn and Ikeda, 1995). We observed Na^+ influx only in the absence of K^+_o (but despite the presence of K^+_i). However, block of I_{DR} by Na^+_o was seen in mixtures of K^+_o and Na^+_o

(Figs. 1, 8, 9), indicating that Na^+ can enter and occupy the pore despite the presence of both K_o^+ and K_i^+. In addition, Na^+ permeation was associated with loss of time- and voltage-dependent gating in *Shaker* (Armstrong and Miller, 1990), whereas I_{DR} channels maintained their usual kinetic behavior in Na_o^+, K_o^+, or mixtures of both. In contrast, I_M channels were not blocked by Na_o^+ and did not conduct Na^+ ions, demonstrating that the effects of Na_o^+ on I_{DR} do not reflect a previously unrecognized general property of K^+ channels, and that the results with Na_o^+ were not a peculiarity of our experimental conditions or of this cell type.

Block by Na_o^+ could be important in physiologic conditions, even though I_{DR} channels would not carry a significant Na^+ current. Especially at more negative voltages, Na_o^+ would partially block I_{DR} during repolarization of the action potential and during the afterhyperpolarization following the action potential. It is also worth noting that the outward rectification of the instantaneous I–V curve (Fig. 9), which resembled Goldman-Hodgkin-Katz rectification, was largely caused by block by Na_o^+.

Cs^+ Permeation and Block

Reports of Cs^+ permeation and conductance through K^+ channels are conflicting. Studies of Ca^{2+}-activated K^+ channels reported no Cs^+ permeation (Blatz and Magleby, 1984; Cecchi et al., 1987; Hu et al., 1989). However, measurable Cs^+ currents were observed through sarcoplasmic reticulum K^+ channels (Cukierman et al., 1985), *Helix* A-current (Taylor, 1987), *Shaker* (Heginbotham and MacKinnon, 1993), lymphocyte K^+ channels (Shapiro and DeCoursey, 1991), and the Kv2.1 K^+ channel (De Biasi et al., 1993). In the squid axon, Cs^+ permeation was inferred by reduction of external Cs^+ block by extreme hyperpolarization, and reduction of internal Cs^+ block by extreme depolarization (Adelman and French, 1978; French and Shoukimas, 1985). For both squid axon and *Shaker*, the effective valence of Cs^+ block varied with K^+ and Cs^+ concentration, as though more Cs^+ ions were present in the channel at higher Cs^+ or lower K^+ (Adelman and French, 1978; Wagoner and Oxford, 1987; French and Shoukimas, 1985; Perez-Cornejo and Begenisich, 1994). The $z\delta$'s varied from 0.6 to 1.3, similar to the 0.63 to 0.96 range reported here. Cs^+ affinity was higher for I_{DR} channels than for squid axon and *Shaker* K^+ channels (Adelman and French, 1978; Perez-Cornejo and Begenisich, 1994).

Many studies of Na^+ and Ca^{2+} currents substitute Cs_i^+ for K_i^+ to block K^+ currents. Although Cs^+ conductance was small compared with K^+, significant inward current can be carried by 120 mM Cs_o^+ (Fig. 7). With intracellular Cs^+, time-dependent outward currents were observed that are clearly distinct from the Na^+ and Ca^{2+} currents of bullfrog sympathetic neurons (Jones, 1987). Similar problems occur in other cell types (Hadley and Hume, 1990; Zhu and Ikeda, 1993). Better prevention of K^+ channel current could be accomplished by substituting NMG^+ for K^+ (Jones and Marks, 1989).

I_M

This is the first detailed report of permeation through I_M channels. The selectivity series was similar to I_{DR}, with the exception of the measurable Na^+ permeability and greater Cs^+ conductance of I_{DR} channels. I_M channels had a G_{Rb}/G_K much lower than P_{Rb}/P_K. Neither conductance nor permeability was concentration-dependent in I_M, and no clear anomalous mole fraction effects were observed. Cs_o^+ blocked I_M with higher affinity but similar effective valence, compared with I_{DR}, and did not show concentration dependence in its effective valence of block. Ion permeation and block of I_M channels could be described by a two-barrier one-site model. In sum, although I_M channels were highly selective for K^+, I_M did not show any clear multi-ion behavior. It is possible that multiple ion occupancy of I_M channels only occurs at higher ion concentrations or with different combinations of ions. Nonetheless, the results with I_{DR} show that multi-ion pore behavior in a K^+ channel could be observed in bullfrog sympathetic neurons under our experimental conditions.

General

The whole-cell mode of patch clamp used in these experiments offered several advantages over single-channel recording for studies of ion selectivity. Separation of I_M and I_{DR} was routinely possible (Adams et al., 1982*a*), whereas unambiguous identification of single-channel currents would be difficult in a cell containing at least six macroscopic K^+ currents (Adams et al., 1982*a*; Jones and Adams, 1987; Jones, 1989). In particular, previous studies of single M-channels have produced conflicting results regarding single-channel conductance and kinetic behavior (Owen et al., 1990; Selyanko et al., 1992; Stansfeld et al., 1993; Marrion, 1993). Whole-cell currents were large, and easily measured over wide voltage ranges, allowing the measurement of currents carried by weakly conducting ionic species. Currents were stable over long times, allowing multiple solution exchanges on the same cell. The main disadvantage of studying whole-cell currents was that careful measurements of activation curves were required to show that changes in current amplitude stemmed from effects on channel conductance and not effects on the open probability. Formally, we cannot rule out the possibility that ions affect p(open) without shifting the activation curve, but that seems unlikely.

The side-by-side comparison of two different K^+ currents in the same cell type allowed us to conclude that

the differences found are real, and do not simply reflect differences in experimental conditions or protocols. Perhaps the most surprising result was that I_{DR} channels were blocked by Na_o^+ under physiological ionic conditions, despite resembling other K^+ channels in most aspects of ionic selectivity. Unlike other K^+ channels (including I_{DR}), I_M channels showed no clear evidence of multi-ion pore behavior, and yet were at least 250-fold selective for K^+ over Na^+. It is not possible to conclude from the absence of multi-ion behavior that I_M channels are single-ion pores, but these results do raise the possibility that the mechanisms underlying permeation and selectivity for I_M differ from previously studied K^+ channels.

We thank Drs. R. Cloues and N.V. Marrion for sharing unpublished data.

Supported in part by NIH grant NS 24471 to S.W. Jones, who is an Established Investigator of the American Heart Association. B.M. Block is also supported by a fellowship from an NIH Medical Scientist Training Program.

Original version received 8 June 1995 and accepted version received 4 November 1995.

REFERENCES

Adams, P.R., D.A. Brown, and A. Constanti. 1982*a*. M-currents and other potassium currents in bullfrog sympathetic neurones. *J. Physiol. (Lond.)*. 330:537–572.

Adams, P.R., D.A. Brown, and A. Constanti. 1982*b*. Pharmacologic inhibition of the M-current. *J. Physiol. (Lond.)*. 332:223–262.

Adelman, W.J., Jr., and R.J. French. 1978. Blocking of squid axon potassium channel by external caesium ions. *J. Physiol. (Lond.)*. 276:13–25.

Armstrong, C.M., and C. Miller. 1990. Do voltage-dependent K^+ channels require Ca^{2+}? A critical test employing a heterologous expression system. *Proc. Natl. Acad. Sci. USA*. 87:7579–7582.

Barry, P.H., and J.W. Lynch. 1991. Liquid junction potentials and small cell effects in patch-clamp analysis. *J. Membr. Biol.* 121:101–117.

Bezanilla, F., and C.M. Armstrong. 1972. Negative conductance caused by entry of sodium and cesium ions into the potassium channels of squid axons. *J. Gen. Physiol.* 60:588–608.

Blatz, A.L., and K.L. Magleby. 1984. Ion conductance and selectivity of single calcium-activated potassium channels in cultured rat muscle. *J. Gen. Physiol.* 84:1–23.

Block, B.M., and S.W. Jones. 1995. Ion permeation in delayed rectifier and M-type potassium currents in bullfrog sympathetic neurons. *Biophys. J.* 68:A42 (Abstr.)

Brüggemann, A., L.A. Pardo, W. Stühmer, and O. Pongs. 1993. *Ether-á-go-go* encodes a voltage-gated channel permeable to K^+ and Ca^{2+} and modulated by cAMP. *Nature (Lond.)*. 365:445–448.

Callahan, M.J., and S.J. Korn. 1994. Permeation of Na^+ through a delayed rectifier K^+ channel in chick dorsal root ganglion neurons. *J. Gen. Physiol.* 104:747–771.

Campbell, D.L., R.L. Rasmusson, and H.C. Strauss. 1988. Theoretical study of the voltage and concentration dependence of the anomalous mole fraction effect in single calcium channels. New insights into the characterization of multi-ion channels. *Biophys. J.* 54:945–954.

Cecchi, X., D. Wolff, O. Alvarez, and R. Latorre. 1987. Mechanism of Cs^+ blockade in a Ca^{2+}- activated K^+ channel from smooth muscle. *Biophys. J.* 52:707–716.

Cukierman, S., G. Yellen, and C. Miller. 1985. The K^+ channel of sarcoplasmic reticulum: A new look at Cs^+ block. *Biophys. J.* 48: 477–484.

De Biasi, M., J.A. Drewe, G.E. Kirsch, and A.M. Brown. 1993. Histidine substitution identifies a surface position and confers Cs^+ selectivity on a K^+ pore. *Biophys. J.* 65:1235–1242.

Eisenman, G., R. Latorre, and C. Miller. 1986. Multi-ion conductance in the high-conductance Ca^{2+}-activated K^+ channel from skeletal muscle. *Biophys. J.* 50:1025–1034.

Fabiato, A., and F. Fabiato. 1979. Calculator programs for computing the composition of the solutions containing multiple metals and ligands used for experiments in skinned muscle cells. *J. Physiol. (Paris)*. 75:463–505.

French, R.J., and J.J. Shoukimas. 1985. An ion's view of the potassium channel. The structure of the permeation pathway as sensed by a variety of blocking ions. *J. Gen. Physiol.* 85:669–698.

Hadley, R.W., and J.R. Hume. 1990. Permeability of time dependent K^+ channel in guinea pig ventricular myocytes to Cs^+, Na^+, NH_4^+, and Rb^+. *Am. J. Physiol.* 259:H1448–H1454.

Hagiwara, S., S. Miyazaki, S. Krasne, and S. Ciani. 1977. Anomalous permeabilities of the egg cell membrane of a starfish in K^+-Tl^+ mixtures. *J. Gen. Physiol.* 70:269–281.

Hagiwara, S., and K. Takahashi. 1974. The anomalous rectification and cation selectivity of the membrane of a starfish egg cell. *J. Membr. Biol.* 18:61–80.

Hamill, O.P., A. Marty, E. Neher, B. Sakmann, and F.J. Sigworth. 1981. Improved patch-clamp techniques for high resolution current recording from cells and cell-free membrane patches. *Pflüg. Arch.* 391:85–100.

Heginbotham, L., and R. MacKinnon. 1993. Conduction properties of the cloned *Shaker* K^+ channel. *Biophys. J.* 65:2089–2096.

Hille, B. 1973. Potassium channels in myelinated nerve. Selective permeability to small cations. *J. Gen. Physiol.* 61:669–686.

Hille, B. 1992. Ionic Channels of Excitable Membranes. 2nd ed. Sinauer Associates Inc., Sunderland, MA. 607 pp.

Hille, B., and W. Schwartz. 1978. Potassium channels as multi-ion single-file pores. *J. Gen. Physiol.* 72:409–442.

Hodgkin, A.L., and R.D. Keynes. 1955. The potassium permeability of a giant nerve fibre. *J. Physiol. (Lond.)*. 128:61–88.

Hu, S.L., Y. Yamamoto, and C.Y. Kao. 1989. Permeation, selectivity and blockade of the Ca^{2+} activated potassium channel of the guinea pig taenia coli myocyte. *J. Gen. Physiol.* 94:849–862

Jones, S.W. 1987. Sodium currents in dissociated bull-frog sympathetic neurones. *J. Physiol. (Lond.)*. 389:605–627.

Jones, S.W. 1989. On the resting potential of isolated frog sympathetic neurons. *Neuron*. 3:153–161.

Jones, S.W. 1991. Time course of receptor-channel coupling in frog

sympathetic neurons. *Biophys. J.* 60:502–507.

Jones, S.W., and P.R. Adams. 1987. The M-current and other potassium currents of vertebrate neurons. *In* Neuromodulation. L.K. Kaczmarek, and I.B. Levitan, editors. Oxford University Press, New York. 159–186.

Jones, S.W., and T.N. Marks. 1989. Calcium currents in bullfrog sympathetic neurons. I. Activation kinetics and pharmacology. *J. Gen. Physiol.* 94:151–167.

Kirsch, G.E., J.M. Pascual, and C.-C. Shieh. 1995. Functional role of a conserved aspartate in the external mouth of voltage-gated potassium channels. *Biophys. J.* 68:1804–1813.

Korn, S.J., and S.R. Ikeda. 1995. Permeation selectivity by competition in a delayed rectifier potassium channel. *Science (Wash. DC).* 269:410–412

Kuffler, S.W., and T.J. Sejnowski. 1983. Peptidergic and muscarinic excitation at amphibian sympathetic synapses. *J. Physiol. (Lond.).* 341:257–278.

Ludwig, J., H. Terlau, F. Wunder, A. Brüggemann, L.A. Pardo, A. Marquardt, W. Stühmer, and O. Pongs. 1994. Functional expression of a rat homologue of the voltage gated *ether-á-go-go* potassium channel reveals differences in selectivity and activation kinetics between the *Drosophila* channel and its mammalian counterpart. *EMBO (Eur. Mol. Biol. Organ.) J.* 13:4451–4458.

Marrion, N.V. 1993. Selective reduction of one mode of M-channel gating by muscarine in sympathetic neurons. *Neuron.* 11:77–84.

Neher, E. 1992. Correction for liquid junction potentials in patch clamp experiments. *Methods Enzymol.* 207:123–31.

Owen, D.G., S.J. Marsh, and D.A. Brown. 1990. M-current noise and putative M-channels in cultured rat sympathetic ganglion cells. *J. Physiol. (Lond.).* 431:269–290.

Perez-Cornejo, P., and T. Begenisich. 1994. The multi-ion nature of the pore in *Shaker* K^+ channels. *Biophys. J.* 66:1929–1938.

Reuter, H., and C.F. Stevens. 1980. Ion conductance and ion selectivity of potassium channels in snail neurons. *J. Membr. Biol.* 57: 103–118.

Selyanko, A.A., C.E. Stansfeld, and D.A. Brown. 1992. Closure of potassium M-channels by muscarinic acetylcholine-receptor stimulants requires a diffusible messenger. *Proc. R. Soc. Lond. B* 250: 119–125.

Selyanko, A.A., J.A. Zidichouski, and P.A. Smith. 1990. A muscarine sensitive, slow, transient outward current in frog autonomic neurones. *Brain Res.* 524:236–243.

Shapiro, M.S., and T.E. DeCoursey. 1991. Selectivity and gating of the type L potassium channel in mouse lymphocytes. *J. Gen. Physiol.* 97:1227–1250.

Stansfeld, C.E., S.J. Marsh, A.J. Gibb, and D.A. Brown. 1993. Identification of M-channels in outside-out patches excised from sympathetic ganglion cells. *Neuron.* 10:639–654.

Tabcharani, J.A., and S. Misler. 1989. Ca^{2+}-activated K^+ channel in rat pancreatic islet B cells: Permeation, gating, and blockade by cations. *Biochim. Biophys. Acta.* 982:62–72.

Taylor, P.S. 1987. Selectivity and patch measurements of A-current channels in *Helix aspersa* neurones. *J. Physiol. (Lond.).* 388:437–447.

Thévenod, F., and S.W. Jones. 1992. Cadmium block of calcium current in frog sympathetic neurons. *Biophys. J.* 63:162–168.

Wagoner, P.K., and G.S. Oxford. 1987. Cation permeation through the voltage-dependent potassium channel in the squid axon. Characteristics and mechanisms. *J. Gen. Physiol.* 90:261–290.

Woodhull, A.M. 1973. Ionic blockage of sodium channels in nerve. *J. Gen. Physiol.* 61:687–708.

Yellen, G. 1984. Ionic permeation and blockade in Ca^{2+}-activated K^+ channels of bovine chromaffin cells. *J. Gen. Physiol.* 84:157–186.

Zhu, Y., and S.R. Ikeda. 1993. Anomalous permeation of Na^+ through a putative K^+ channel in rat superior cervical ganglion neurones. *J. Physiol. (Lond.).* 468:441–461.